# Improved coronary artery calcium (CAC) detection in conventional CT with deep-learning image de-blurring

Wülker, Christian; van der Werf, Niels R.; Schnellbächer, Nikolas D.; Greuter, Marcel J.W.; Grass, Michael

*Published in:*
Medical Imaging 2024

*DOI:*
10.1117/12.3006693

# Improved coronary artery calcium (CAC) detection in conventional CT with deep-learning image de-blurring

Christian Wülker[a], Niels R. van der Werf[b], Nikolas D. Schnellbächer[a], Marcel J. W. Greuter[c], and Michael Grass[a]

[a]Philips Innovative Technologies, Hamburg, Germany
[b]Philips Healthcare, Eindhoven, The Netherlands
[c]University Medical Center Groningen, The Netherlands

## ABSTRACT

We investigated the impact of a CNN-based deep-learning (DL) image de-blurring algorithm on coronary artery calcium (CAC) detection performance in conventional CT imaging. Our approach comprises first de-noising the image with a state-of-the-art CNN-based image de-noising algorithm. With improved SNR, it is then possible to sharpen the image with a CNN-based image de-blurring algorithm. We train such networks using natural images, *i.e.*, a large set of diverse photographs. The de-noising strength in the final image can be adjusted by blending back the estimated noise from the first step to the desired degree. To assess the impact of the de-blurring algorithm, we scanned an anthropomorphic phantom containing 100 small calcifications on a CT system using a CAC scoring protocol. Data were acquired at clinical and high dose, and subsequently reconstructed with and without the DL de-blurring algorithm, using 25% of the maximum de-noising strength. For each small CAC, detectability was defined as the ability to calculate an Agatston score (at least 3 adjacent voxels exceeding 130 HU). For the high dose scans, CAC detectability increased from 39% for the standard reconstruction to 49% with de-blurring. The same 39% CAC detectability at high dose without de-blurring was obtained with routine dose with de-blurring. In this work, we also show some visual impressions of applying our DL de-blurring method to clinical cardiac data.

**Keywords:** Computed tomography (CT), image quality, machine learning, deep learning, de-blurring, de-noising, coronary artery calcium, clinical task-based metrics

## 1. INTRODUCTION

Clinical CT imaging is susceptible to noise and system blur, both of which can impair the readability and quality of CT images. While noise in CT is caused by statistical effects in physical signal generation and data acquisition, CT system blur can be seen as an inherent resolution loss and concomitant reduced perceived sharpness resulting from various physical effects such as detector blur or source blur due to focal spot shape/size, among others[*]. Because of the inherent blur in CT systems, fine image detail might be lost and hamper timely and correct diagnosis. This is particularly relevant when a clinical task involves the detection of small objects, such as in coronary artery calcification (CAC) detection. Moreover, CT system blur can result in images that are perceived as unsharp/blurred, with correspondingly longer and more exhausting image reading time.

In clinical CT imaging, keeping the radiation exposure as low as reasonably achievable (ALARA) is a guideline commonly agreed upon. This, however, comes at the cost of higher noise levels in the reconstructed images, which explains the need for fast high-quality image de-noising algorithms. Convolutional neural networks (CNNs) are a powerful machine-learning technique well suited to perform image de-noising in various medical image domains. This type of neural network has been used in the recent past to successfully establish advanced CT image de-noising methods in clinical practice (see, for example, [1]). CT image de-blurring using such novel deep-learning (DL) technology, on the other hand, has only started to being established in practice (see, *e.g.*, [2]).

Please address all correspondence to christian.wuelker@gmail.com
[*]Note that we are not dealing with motion blur or other such non-deterministic effects in this work.

Medical Imaging 2024: Physics of Medical Imaging, edited by Rebecca Fahrig, John M. Sabol, Ke Li,
Proc. of SPIE Vol. 12925, 129252B · © 2024 SPIE · 1605-7422
doi: 10.1117/12.3006693

In this work, we investigate the impact of a CNN-based DL de-blurring algorithm on the performance of CAC detection. For this, CT scans were made of a one-of-a-kind anthropomorphic phantom containing 100 small cylindrical CACs of different sizes and densities to allow for a CAC detection analysis. This phantom has previously been used to compare CAC detection performance for different CT systems, including novel photon-counting CT [3, 4]. We use a state-of-the-art CNN-based CT image de-noising algorithm to de-noise the initial reconstructed images. After that, we apply a generic CNN-based de-blurring algorithm trained on natural images (various photographs) to these de-noised images. In a final step, the estimated noise from the first step can be blended back to the de-blurred images to the desired degree. This method is different from other DL approaches currently being investigated, which try to solve the de-noising and de-blurring problem simultaneously using a single neural network (cf. [5]).

Notably, this work can also be seen as part of a larger endeavor to rely more on clinical task-based metrics when evaluating the performance of DL algorithms in medical image formation, instead of relying solely on standard metrics such as peak SNR (PSNR) and structural similarity index (SSIM) with their well-known shortcomings.

## 2. MATERIALS AND METHODS

### 2.1 Phantom and phantom data acquisition

An anthropomorphic chest phantom (QRM Thorax, QRM Inc., Möhrendorf, Germany) was scanned on a commercially available dual-layer CT system (Spectral CT 7500, Philips Healthcare). At the center of the phantom, an insert was positioned which contained 100 small cylindrical calcifications. The calcifications were of different sizes (0.5-2.0 mm in diameter and length) and densities (90-540 mg hydroxyapatite per cc). Data were acquired and reconstructed using a routine clinical protocol (axial scan, 120 kVp tube voltage, 128 $\times$ 0.625 mm collimation, 0.27 s rotation time, 220 mm field-of-view (FOV), 512 $\times$ 512 matrix size). Reconstruction was done using filtered back-projection (FBP) with Philips standard resolution C filter. We did not use any image de-noising at this stage, for this is a pre-processing step in our DL de-blurring framework (see below). Two radiation dose levels were used, a clinical dose level (tube current time product of 51.4 mAs) and a high dose level (269.5 mAs, respectively). The slice thickness and increment were 1 mm and 0.5 mm, respectively. To account for inter-scan variation, the phantom was scanned five times with small manual repositioning (approximately 2 degrees rotation and 2 mm translation) of the phantom in-between scans.

### 2.2 Clinical cardiac data

We also tested our DL de-blurring method by applying it to a clinical routine cardiac scan. In particular, a clinical cardiac scan was performed with a conventional CT scanner with dual-focal spot and 128 row detector (iCT, Philips Healthcare) at 100 kVp and 922 mA tube current and 0.27 s rotation time, resulting in a CTDIvol value of 17 mGy. Data were acquired with ECG gating and reconstructed at the 75% phase of the heart cycle with a patient heart rate of 49 bpm. Scan collimation was set to 128 $\times$ 0.625 mm = 80 mm scan coverage, the scan itself performed in prospectively-gated axial scan mode (step and shoot cardiac) using two shots to cover the full heart of the patient. Image reconstruction was done using FBP on a 512 $\times$ 512 matrix with Philips standard resolution cardiac CC reconstruction kernel at 0.8 mm slice thickness and 0.4 mm slice increment and with a FOV of 250 mm. As with the phantom data, we did not use any image de-noising on the input images for de-blurring, for this is taken care of by our DL de-blurring framework.

### 2.3 DL de-noising algorithm

In this work, we use a state-of-the-art CNN-based CT image de-noising algorithm similar to the one previously described in [6], but re-trained it for a smaller cardiac FOV. The network was trained using data from five clinical CT body scans. Advanced low-dose simulation [7] was applied to the acquired raw data to simulate a 25% dose level from the acquired 100% dose by artificially reducing the tube current. Images were reconstructed with FBP using the acquired 100% and simulated 25% dose, not using image de-noising. The network was trained to estimate the noise from the 25% dose input images. For more details on the training (optimizer, data augmentation, etc.) refer to [6].

### 2.4 DL de-blurring algorithm

For the DL de-blurring algorithm, we used a similar neural network architecture as for the de-noising. Specifically, the network architecture was a 2D bias-free feed-forward CNN as described in [8], which was trained in a supervised manner using an adaptive moment estimation (Adam) optimizer [9] and the mean absolute error (L1) as the loss function. The CNN architecture we used had 16 convolutional layers with 5 $\times$ 5 kernel size and without padding (so-called valid convolutions), each followed by a leaky rectified linear unit (ReLU) as nonlinearity, plus one final layer with a 1 $\times$ 1 convolution. The number of channels between the convolutional layers was set to 64. We trained the network using a set of several hundreds of natural images (*i.e.*, diverse photographs) called DIV2K[†] [10]. The input images were generated by first down-sampling the images to half the size in each direction, followed by up-sampling them to the original size using bicubic interpolation, and then applying Gaussian blur with the standard deviation (sigma) equal to 1.15 pixels. The network was trained to predict the difference between such a blurred input image to its original counterpart. Training was done in a patch-wise manner using a patch size of 100 $\times$ 100 pixels. Random flipping in both directions was done on-the-fly during training for data augmentation. The learning rate was set to $10^{-4}$. We trained the network with a minibatch size of 100 for a fixed number of iterations, chosen such that convergence was observed.

### 2.5 Image processing

The application of our DL image de-blurring method was similar with both phantom and clinical data. In a first step, we applied the CNN-based de-noising algorithm described in Section 2.3 to estimate the noise in the respective input images. The noise was then subtracted to yield the de-noised input images for the DL de-blurring algorithm of Section 2.4. In a final step, a fraction of the noise estimated in the first step was blended back to the de-blurred images to achieve a certain de-noising level. We applied the same de-noising to the images with and without de-blurring to allow for a fair comparison. Specifically, we blended back 75% of the noise estimated in each image with the phantom data, resulting in a de-noising strength of 25%, and 50% of the noise in each image reconstructed from the clinical cardiac data, resulting in a 50% de-noising strength.

### 2.6 Phantom image analysis

CAC detection performance was assessed using a previously validated in-house developed Python script [11]. For each CAC, detectability was defined as the ability to calculate an Agatston score. Specifically, this meant a minimum of 3 adjacent voxels (area larger than 0.5 mm$^2$) exceeding the Agatston scoring threshold of 130 Hounsfield units (HU). Total CAC detectability was defined as the percentage of detected CACs for all five repeated scans for each dose level, respectively.

## 3. RESULTS

### 3.1 Results based on phantom data

Representative images of the phantom are shown in Figure 1. For the reference acquisition (routine clinical dose, without de-blurring), 37% of the calcifications were detected. With increased radiation dose, this figure increased to 39% CAC detection. With the de-blurring algorithm applied, CAC detection increased to 39% for clinical and 49% for high radiation dose, respectively.

### 3.2 Images based on clinical cardiac data

Figure 2 shows exemplary results of our DL de-blurring method as applied to the clinical cardiac CT scan described in Section 2.2. First, we show images from the conventional processing, where apart from the standard cardiac CT reconstruction only the CNN-based de-noising was active. Next to these, we add the DL de-blurring CNN to the full image reconstruction chain resulting in a distinctly sharpened overall image appearance without amplifying or sharpening the noise.

[†] https://data.vision.ee.ethz.ch/cvl/DIV2K/

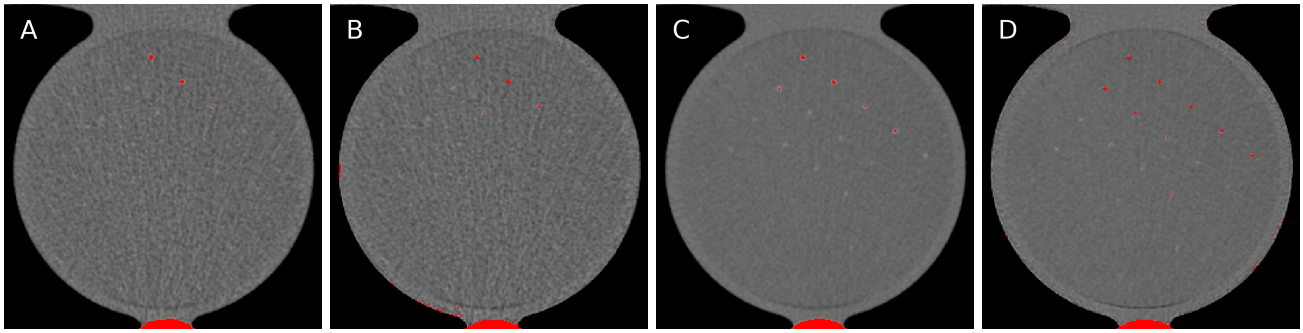


**Figure 1.** Representative images of the CAC phantom with voxels exceeding the Agatston scoring threshold of 130 HU labeled in red. The slice shown contains the 25 smallest (0.5-1.0 mm) and highest density (240-540 mg hydroxyapatite/cc) calcifications. Results are shown for **(A)** clinical dose and standard reconstruction, **(B)** clinical dose and DL de-blurred reconstruction, **(C)** high dose and standard reconstruction, and **(D)** high dose and DL de-blurred reconstruction. All images are shown at a level of 90 HU and with a window width of 750 HU.

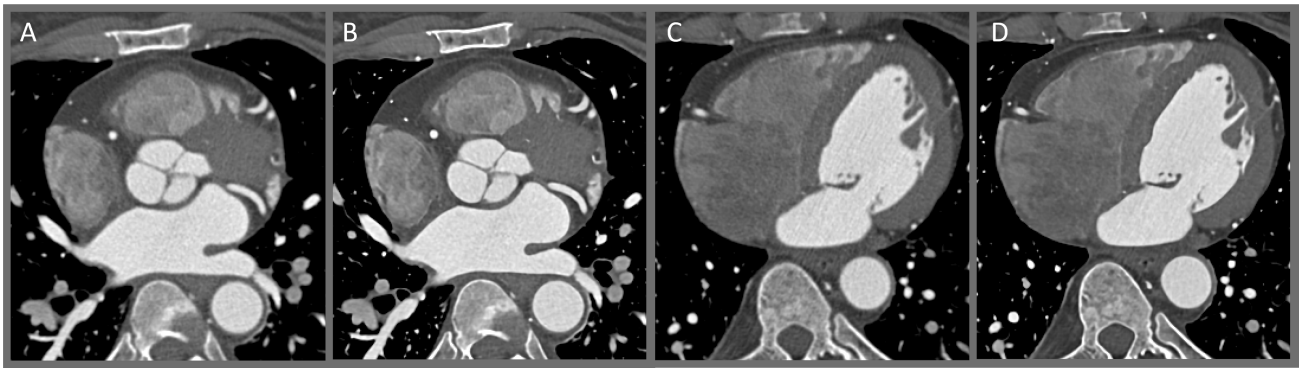


**Figure 2.** Exemplary axial images from a gated cardiac CT acquisition shown at two different axial slice locations of the human heart. **A** and **B** depict the same axial cross section with the conventional cardiac reconstruction shown in A compared to the DL-based image de-blurring method shown in B. Both images are windowed to a level of 200 HU and a window width of 1250 HU. **C** and **D** show a lower axial slice. Again, conventional processing in C is compared to the processing with DL image de-blurring active as shown in D. Here both images are shown at a level of 250 HU and with a window width of 1200 HU.

## 4. DISCUSSION AND CONCLUSION

We investigated the impact of a generic CNN-based DL image de-blurring algorithm on CAC detection and perceived image sharpness. The quantitative figures for CAC detection performance in the dedicated phantom experiment show that such technology is indeed capable of improving image quality, measured in terms of a clinical task-based metric at clinically relevant dose, thereby offering opportunities to reduce radiation dose. One of the major advantages of our approach is that the de-blurring is applied in combination with a high-performance CNN-based DL image de-noising algorithm. This allowed us to revert CT system blur without amplifying or sharpening the noise, while at the same time achieve the desired SNR level by blending back only a fraction of the noise estimated in the images before de-blurring. Images of our DL de-blurring method applied to clinical cardiac images demonstrate the capability to visually improve the perceived image sharpness of CT images, potentially resulting in improved diagnostic quality as well as faster and less exhausting image reading in clinical practice.

A current imperfection of our method is that it resulted in a small edge enhancement, in particular around the calcifications in the phantom (note also the small areas labeled in red at the edge of the phantom insert in Fig. 1 (B), for example). This can be attributed to the fact that the Gaussian blurring we used to train the de-blurring network does not yet accurately represent the blur inherent to a CT system. While such edge enhancements do not impair the detectability of the calcifications, they may impair quantification accuracy.

Our plan is to address this current shortcoming, *e.g.*, by introducing an additional nonlinear processing step or adapting network training in a suitable way.

## REFERENCES


[1] Greffier, J., et al., "Impact of an artificial intelligence deep-learning reconstruction algorithm for CT on image quality and potential dose reduction: A phantom study," *Med. Phys.* **49**(8), 5052–5063 (2022).

[2] Lee, T.-C., et al., "Deep learning enabled wide-coverage high-resolution cardiac CT," in [*7th International Conference on Image Formation in X-Ray Computed Tomography*], Stayman, J. W., ed., *Proc. SPIE* **12304**, 123041O (2022).

[3] Groen, J. M., et al., "Calcium score of small coronary calcifications on multidetector computed tomography: Results from a static phantom study," *Eur. J. Radiol.* **82**(2), e58–e63 (2013).

[4] van der Werf, N. R., et al., "Coronary calcium scoring potential of large field-of-view spectral photon-counting CT: A phantom study," *Eur. Radiol.* **32**(1), 152–162 (2022).

[5] Yuan, Y., et al., "Deep learning CT image restoration using system blur models," in [*Medical Imaging: Physics of Medical Imaging*], Yu, L., Fahrig, R., and Sabol, J. M., eds., *Proc. SPIE* **124634**, 124634J (2023).

[6] Wülker, C., et al., "Filter-independent CNN-based CT image denoising," *arXiv:2310.16846 Proc. Fully3D* (2023).

[7] Žabić, S., et al., "A low dose simulation tool for CT systems with energy integrating detectors," *Med. Phys.* **40**(3), 031102 (2013).

[8] Mohan, S., et al., "Robust and interpretable blind image denoising via bias-free convolutional neural networks," *arXiv:1906.05478* (2020).

[9] Kingma, D. P. and Ba, J., "Adam: A method for stochastic optimization," *arXiv:1412.6980* (2017).

[10] Agustsson, E. and Timofte, R., "NTIRE 2017 challenge on single image super-resolution: Dataset and study," in [*2017 IEEE Conference on Computer Vision and Pattern Recognition Workshops (CVPRW)*], 1122–1131 (2017).

[11] van Praagh, G. D., et al., "Fully automated quantification method (FQM) of coronary calcium in an anthropomorphic phantom," *Med. Phys.* **48**(7), 3730–3740 (2021).